Catalysis Science & Technology

ROYAL SOCIETY OF CHEMISTRY

PAPER

View Article Online
View Journal | View Issue

Cite this: *Catal. Sci. Technol.*, 2026, **16**, 1983

Direct synthesis of methyl acetate and acetic acid from syngas over tandem catalysts composed of a Cu-based catalyst and a Cu-exchanged mordenite zeolite

Katsuya Shimura, * Isao Nakamura and Tadahiro Fujitani

Direct conversion of syngas to methyl acetate (MA) and acetic acid (AA) was investigated using a tandem catalyst system combining Cu-based catalysts for methanol synthesis and mordenite (MOR) zeolite for dimethyl ether (DME) carbonylation. The catalysts were loaded as separate layers in a fixed-bed flow reactor and used to convert syngas to MA and AA *via* methanol and DME at 230 °C and 5 MPa. Combination of a Cu catalyst with unmodified MOR afforded DME with high selectivity (87%), but the selectivity for MA was low at 2%; however, replacement of the zeolite with a Cu ion-exchanged MOR increased the total selectivity for MA and AA thirtyfold without affecting hydrocarbon formation. A Cu ion-exchanged MOR with both moderate Cu loading and SiO_2/Al_2O_3 ratio showed the highest activity, indicating that Cu ions and Brønsted acid sites are both essential for efficient DME carbonylation. Characterization of the tandem catalysts revealed that Cu^+ ions present within the eight-membered ring channels of MOR enhanced CO adsorption and insertion into DME, boosting catalytic activity. The effects of reaction temperature, the weight ratio of the two catalyst layers and the gas hourly space velocity were also investigated, and the maximum total selectivity of MA and AA reached 93.7%.

Received 29th January 2026,
Accepted 23rd February 2026

DOI: 10.1039/d6cy00105j

rsc.li/catalysis

1. Introduction

To realize a carbon-neutral society, it will be crucial to establish processes for producing liquid fuels and chemicals from syngas (a mixture of H_2, CO, and CO_2), which can be obtained by gasifying biomass[1] and waste plastics.[2] Among existing syngas conversion processes, methanation,[3] methanol synthesis,[4] and Fischer–Tropsch synthesis[5] are already at the practical stage. However, converting syngas into C_2 oxygenates such as ethanol and acetic acid (AA) remains challenging. Ethanol is widely used as a solvent, fuel, and fuel additive, as well as a platform molecule for producing value-added chemicals. In recent years, methods for converting ethanol into various chemicals and fuels, such as ethylene, propylene, butadiene, isobutene, gasoline, and 1-butanol, have been extensively studied and are becoming well established.[6–8] Therefore, developing efficient processes for converting syngas into C_2 oxygenates would be a major step toward realizing a carbon-recycling society.

Four types of heterogeneous catalysts have been extensively studied for the direct conversion of syngas into C_2 oxygenates using a single catalyst: rhodium-based catalysts, modified methanol synthesis catalysts, modified Fischer–Tropsch synthesis catalysts, and molybdenum-based catalysts.[9–11] Rhodium-based catalysts exhibit high total C_2 oxygenate selectivity, often exceeding 70%, but their high cost and limited availability hinder commercialization. The other three types are much cheaper, but their C_2 oxygenate selectivity is typically low because of the formation of byproducts such as methanol, CO_2, and hydrocarbons. The conversion of syngas into C_2 oxygenates is a highly complex reaction involving numerous elementary steps, including H_2 dissociation, CO dissociative and non-dissociative adsorption, formation of CH_xO and CH_y intermediates, and C–C coupling of these intermediates.[12] For selective synthesis of C_2 oxygenates, the quality and quantity of active sites for CO dissociative and non-dissociative adsorption must be precisely controlled, which makes catalyst design very difficult. Consequently, no practical catalysts with high selectivity, stability, and low cost have yet been developed for this reaction.

Syngas can also be converted into C_2 oxygenates indirectly *via* a sequence of reactions: methanol synthesis, methanol dehydration to dimethyl ether (DME), carbonylation of DME to methyl acetate (MA) and hydrogenation of MA to ethanol.[13] Ethanol is also produced by carbonylation of

Research Institute for Chemical Process Technology, National Institute of Advanced Industrial Science and Technology (AIST), 1-1-1 Higashi, Tsukuba, Ibaraki 305-8565, Japan. E-mail: katsuya-shimura@aist.go.jp

methanol to AA and the successive hydrogenation. Among these steps, carbonylation of DME to MA (methanol to AA) is the most important for efficient C_2 oxygenate production.[13] A major breakthrough in DME carbonylation using heterogeneous catalysts was reported in 2006 by Cheung *et al.*, who found that mordenite (MOR) zeolite exhibited excellent selectivity (99%) at 150–190 °C for this reaction.[14,15] The DME carbonylation rate was found to be proportional to the number of O–H groups acting as Brønsted acid sites (BASs) within the eight-membered ring (8-MR) channels of the zeolite, indicating that the reaction proceeds predominantly within the 8-MR channels of MOR.[16] Later theoretical calculations[17–20] and experimental studies[21–24] by other groups revealed that the high catalytic activity of MOR, which actually has both 8-MR and 12-MR channels, arises from the distinct roles of these two channels: the 8-MR channels serve as active centers of DME carbonylation because of their low activation barrier and CO aggregation property around active sites, while the 12-MR channels provide pathways for reactant and product transport. To improve the MOR catalytic performance, modifications with transition metals such as Cu,[25–27] Fe,[28] Co,[29] Zn,[30] Ag,[31] and Pt (ref. 32) have been extensively investigated, with Cu identified as the most effective promoter.[33] Additionally, selective removal or passivation of BASs in the 12-MR channels has been shown to suppress coke formation and extend catalyst lifetime.[34–37] Fan *et al.* have reported a MOR catalyst capable of stable MA production with high selectivity (>98%) out to 520 h, demonstrating the potential of MOR-catalyzed DME carbonylation for practical applications.[38]

Direct conversion of syngas into C_2 oxygenates using tandem catalysts has also been reported. In this approach, multiple catalysts promoting methanol synthesis, methanol dehydration to DME, DME carbonylation to MA, and MA hydrogenation to ethanol are loaded into a single reactor in separate layers, enabling syngas conversion to C_2 oxygenates *via* relay catalysis. The first studies on C_2 oxygenate synthesis using tandem catalysts was reported by Tsubaki's group, who achieved selective synthesis of methanol and ethanol from DME and syngas by combining a zeolite catalyst for DME carbonylation with a Cu/ZnO catalyst for MA hydrogenation.[39–42] Several other groups have also reported direct syngas-to-ethanol conversion using tandem catalysis.[12,43–49] In particular, a triple-tandem catalyst system composed of $CuZnAlO_x$/γ-Al_2O_3, pyridine-modified H-MOR zeolite, and $Cu_1Zn_2AlO_x$ exhibited excellent performance, achieving 52% CO conversion and 62% ethanol electivity (excluding CO_2).[48] However, studies on syngas conversion to C_2 oxygenates using tandem catalysts remain limited, and the optimal catalyst combinations and reaction conditions have not yet been fully clarified. Therefore, systematic investigation is needed to improve the efficiency of syngas conversion to C_2 oxygenates *via* tandem catalysis.

In this study, the direct conversion of syngas to MA and AA was investigated using tandem catalysts composed of a Cu-based methanol synthesis catalyst and a metal ion-exchanged zeolite catalyst. The effects of zeolite type, amount and type of exchanged metal ions, and reaction conditions on C_2 oxygenate selectivity were examined in detail, revealing that all these factors markedly influenced product selectivity. The combination of a $CuMgAlO_x$ catalyst and a Cu-exchanged MOR at a weight ratio of 1 : 6, operated at 230 °C and a gas hourly space velocity of 3.4 L g^{-1} h^{-1} exhibited the best performance, achieving a total MA and AA selectivity of 93.7% at 2.8% CO conversion.

We have paid special attention to clarifying the loading effects of metal ions on MOR zeolite. As listed in Table S1, the unmodified zeolite[43,47] and MOR, which eliminated BASs in 12-MR,[12,46,48,49] have been frequently employed as the DME carbonylation catalyst for the conversion of syngas to MA and AA. However, there were few examples to use metal ion-exchanged MOR zeolites as the DME carbonylation catalyst.[44,45] In the tandem catalytic system, not only DME and CO but also H_2 and H_2O coexist during the reaction. Thus, it is expected that the loading effect of metal ions is quite different from that of the conventional DME carbonylation system using only CO and DME as the reactants. We found that Cu-MOR showed more than 30 times higher activity than the unmodified MOR in the tandem catalytic system, although it was reported that Cu ion-exchange only increased the catalytic activity for DME carbonylation by several times under water-free conditions.[13] This result clearly shows the usefulness of Cu ion-exchange in tandem catalytic systems.

We have also focused on clarifying the structure and roles of active Cu species of the Cu-MOR zeolite catalyst. Cu has been widely confirmed to work as the effective promoter for the MOR-catalyzed DME carbonylation.[13] However, the oxidation state and roles of active Cu species are still unclear. Three different species, *i.e.*, Cu^{2+},[33] Cu^{+},[25,45] and Cu metal,[27,50,51] have been proposed as the active Cu species, and no consensus has been reached. The present work strongly suggests that Cu^{+} ions within 8-MR channels work as the active sites for DME carbonylation.

2. Experimental

2.1. Catalyst preparation

Mixed oxides containing Cu, Mg, and Al (denoted hereafter as CMA) or Cu, Mg, Y, and Al (denoted hereafter as CMYA) were used as Cu-based methanol synthesis catalysts. All reagents used for preparation of the Cu catalysts were purchased from Fujifilm Wako Pure Chemical Corporation. Both catalysts were prepared by a coprecipitation method. For preparation of the CMA catalyst, $Cu(NO_3)_2{\cdot}3H_2O$ (99.9%, 19.328 g), $Mg(NO_3)_2{\cdot}6H_2O$ (99.0+%, 16.923 g), and $Al(NO_3)_3{\cdot}9H_2O$ (99.9%, 20.257 g) were dissolved in 200 mL of deionized water at a Cu/Mg/Al molar ratio of 40/33/27. The precipitant solution was prepared by dissolving NaOH (97.0+%, 11.999 g) and Na_2CO_3 (99.8+%, 11.447 g) in 200 mL of deionized water. The metal precursor solution was then added to the precipitant solution under vigorous

stirring (15 000 rpm) using a homogenizer at room temperature, at an addition rate of 10 mL min^{-1} controlled by a tube pump. After addition, the slurry was aged at 80 °C for 24 h, filtered, washed three times with distilled water, and dried at 60 °C for 24 h. The resulting powder was calcined in air at 400 °C for 3 h. The CMYA catalyst was prepared following the same procedure, except that $Y(NO_3)_3{\cdot}6H_2O$ (99.9%) was used as the Y source and a Cu/Mg/Y/Al molar ratio of 40/25/8/27 was used.

Metal-loaded zeolite catalysts were prepared using an ion-exchange method. The zeolite powders used were HSZ-640HOA (MOR, SiO_2/Al_2O_3 = 18; Tosoh), HSZ-620HOA (MOR, SiO_2/Al_2O_3 = 15; Tosoh), HSZ-660HOA (MOR, SiO_2/Al_2O_3 = 30; Tosoh), HSZ-690HOA (MOR, SiO_2/Al_2O_3 = 240; Tosoh), JRC-Z-HM90 (MOR, SiO_2/Al_2O_3 = 90; Süd-Chemie), H-CZC-13 (CHA, SiO_2/Al_2O_3 = 26; Clariant), HSZ-720NHA (FER, SiO_2/Al_2O_3 = 18; Tosoh), HSZ-822HOA (ZSM-5, SiO_2/Al_2O_3 = 24; Tosoh), CP814E (Beta, SiO_2/Al_2O_3 = 25; Zeolyst), and HSZ-350HUA (Y, SiO_2/Al_2O_3 = 10; Tosoh). Amorphous SiO_2-Al_2O_3 (ASA, Al_2O_3 28.6%, JRC-SAH-1; JGC Catalysts and Chemicals) was used as a reference sample. The metal precursors used were $Mg(NO_3)_2{\cdot}6H_2O$, $Mn(NO_3)_2{\cdot}6H_2O$, $FeSO_4{\cdot}7H_2O$, $Co(NO_3)_2{\cdot}6H_2O$, $Ni(NO_3)_2{\cdot}6H_2O$, $Cu(NO_3)_2{\cdot}3H_2O$, $Zn(NO_3)_2{\cdot}6H_2O$, and $AgNO_3$, which were purchased from Fujifilm Wako Pure Chemical Corporation. Ion-exchange was performed 1–5 times at 80 °C for 4 h using aqueous metal precursor solutions (metal concentration, 0.1–1 mol L^{-1}; liquid-to-solid ratio, 10 mL g^{-1}). After ion-exchange, the catalyst was recovered by filtration, washed three times with distilled water, dried at 110 °C overnight, and calcined in air at 400 °C for 3 h. The metal ion loading was adjusted by varying the number of ion-exchange cycles and the concentration of the precursor solution. For simplicity, the names of the metal ion-exchanged zeolite catalysts are denoted as M(x)–Z(y), where M and x represent the type and loading amount of the metal ion, respectively, and Z and y represent the zeolite crystal structure and SiO_2/Al_2O_3 ratio, respectively.

2.2. Catalyst characterization

Cu-based methanol synthesis catalysts and metal ion-exchanged zeolite catalysts were characterized by N_2 adsorption–desorption, X-ray diffraction (XRD), inductively coupled plasma atomic emission spectroscopy (ICP-AES), field-emission scanning electron microscopy (FE-SEM), N_2O chemisorption, UV-vis spectroscopy, NH_3 temperature-programmed desorption (NH_3-TPD), H_2 temperature-programmed reduction (H_2-TPR), Fourier transformed infrared (FT-IR) spectroscopy, *in situ* diffuse reflectance infrared Fourier transform spectroscopy (DRIFTS), CO temperature-programmed desorption (CO-TPD) and thermogravimetric analysis (TGA). The detailed characterization information and procedures are presented in the SI.

2.3. Catalytic reaction

Conversion of syngas to MA and AA was performed using a fixed-bed down-flow reactor. Cu-based catalyst and MOR zeolite were granulated into particles with diameters of 0.35–0.71 nm and packed in two layers in the center of the reactor (inner diameter, 17 mm; length, 29 cm) with the Cu-based catalyst (0.50 g) on top and the MOR zeolite (2.0 g) below. The catalysts were reduced in a flow of H_2 (33%)/N_2 (60 mL min^{-1}) at 350 °C for 1 h at atmospheric pressure. After cooling to the reaction temperature, the reactor was pressurized using the back-pressure valve. The reaction was typically performed at 230 °C and 5 MPa for 340 min using a feed gas mixture of CO (33%)/H_2 (150 mL min^{-1}) and N_2 (50 mL min^{-1}). Reaction products were analyzed using two on-line gas chromatographs (GC-2014; Shimazu): one equipped with a thermal conductivity detector and a ShinCarbon ST packed column (2 m × 3 mm, Shinwa Chemical Industries Ltd.) and the other with a flame ionization detector and a TC-BOND Q capillary column (30 m × 0.32 mm, GL Sciences). The carbon mass balance of the products was within 100 ± 5% for most of the catalysts.

3. Results and discussion

3.1. Conversion of syngas to MA and AA using tandem catalysts

The conversion of syngas to MA and AA was examined using CMYA (0.5 g) and Cu(3.1)-MOR(18) (2.0 g) catalysts, either individually or in combination, under a flowing gas mixture of CO (33%)/H_2 (150 mL min^{-1}) and N_2 (50 mL min^{-1}) at 230 °C and 5 MPa (Table 1). When the reaction was performed using only the CMYA catalyst, methanol was produced with a very high selectivity of 98.6% at a CO conversion of 4.3% (entry 1). When H-form MOR(18) zeolite was added downstream of the CMYA catalyst, methanol dehydration occurred on the BASs of MOR, and DME selectivity increased sharply from 0.7% to 86.9% without a marked change of the CO conversion (entry 2). H-MOR(18) also promoted DME carbonylation to MA, but the MA selectivity remained low at 2.1% because of the slow DME carbonylation rate over H-MOR(18). We speculate that water produced by methanol dehydration may poison the active sites on H-MOR for DME carbonylation, resulting in the low catalytic activity.[49] Cu ion exchange of MOR(18) markedly enhanced DME carbonylation, increasing MA selectivity from 2.1% to 60.8% (entry 3). A small amount of AA (selectivity 4.8%) was also observed, likely formed by hydrolysis of MA (CH_3COOCH_3 + $H_2O \rightarrow CH_3COOH + CH_3OH$). Cu-MOR further increased CO_2 selectivity, which was attributed to the water–gas shift reaction ($CO + H_2O \rightarrow CO_2 + H_2$) involving water produced during methanol dehydration. No reaction occurred over Cu-MOR(18) alone under syngas flow (entry 4). These results (entries 1–4) suggested that combined use of CMYA and Cu-MOR(18) as the upper and lower bottom layers, respectively, produced a tandem system able to efficiently convert syngas to MA *via* methanol and DME intermediates.

When the catalyst loading order was reversed, with Cu-MOR(18) on top and CMYA on the bottom, no formation of MA and AA was observed (Table 1, entry 5). Instead,

Table 1 Conversion of syngas to MA and AA over various combinations of CMYA and Cu(3.1)-MOR(18) catalysts[a]

Entry	Catalyst		CO conv. (%)	Selectivity[b] (%)								Yield of MA + AA (%)
	Top layer	Bottom layer		CO_2	CH_4	C_{2-4} HC	C_{5-6} HC	MeOH	EtOH	MA	AA	DME	
1	CMYA	—	4.3	0.4	0.5	0.0	0.0	98.6	0.3	0.0	0.0	0.7	0.00
2	CMYA	H-MOR(18)	4.0	1.7	0.4	0.4	0.0	8.1	0.0	2.1	0.0	86.9	0.08
3	CMYA	Cu(3.1)-MOR(18)	4.9	8.5	0.4	0.5	0.0	3.4	0.0	60.8	4.8	23.7	3.17
4	Cu(3.1)-MOR(18)	—	0.0	0.0	0.0	0.0	0.0	0.0	0.0	0.0	0.0	0.0	0.00
5	Cu(3.1)-MOR(18)	CMYA	2.6	14.5	0.3	3.5	0.0	53.1	0.8	0.0	0.0	25.0	0.00
6	Mixture of CMYA and Cu(3.1)-MOR(18)		1.8	43.0	0.0	48.6[c]	0.0	0.0	0.0	0.0	0.0	0.0	0.00

[a] CMYA 0.5 g, Cu(3.1)-MOR(18) 2.0 g, 230 °C, 5 MPa, 340 min, syngas 150 mL min^{-1}, N_2 50 mL min^{-1}. [b] C_{2-4} HC: hydrocarbons with a carbon number of 2–4, C_{5-6} HC: hydrocarbons with a carbon number of 5–6, MA: methyl acetate, AA: acetic acid. [c] C_2H_6 only.

methanol was the main product, while DME, CO_2, and C_{2-4} hydrocarbons were produced as minor products. This result is reasonable because Cu-MOR(18) alone was inactive for syngas conversion (entry 4), meaning the reaction occurred only over the CMYA catalyst. Consequently, most of the methanol produced over CMYA passed over the second catalyst without further reaction. However, some methanol may have reacted on the acid sites of Cu-MOR(18) located near the CMYA catalyst to form DME and C_{2-4} hydrocarbons. In contrast, the physical mixture of CMYA and Cu-MOR(18) did not produce MA, AA, methanol, or DME, but instead produced ethane and CO_2 (entry 6). A similar observation was reported by Zhou *et al.*, who used $ZnAl_2O_4$ and H-MOR catalysts for methanol synthesis and DME carbonylation, respectively.[43] The cause of the different reactivity of the physically mixed catalysts compared with the layered system is unclear, but it is suspected that MA formed on Cu-MOR may decompose on CMYA to produce C_2H_6 and CO_2.

The time course of CO conversion and product selectivity was examined using a combination of CMYA (0.5 g) and Cu(3.1)-MOR(18) (2.5 g) at 230 °C and 5 MPa (Fig. 1). During the 10 h reaction, CO conversion remained nearly constant at around 3.5%, with no noticeable catalyst deactivation. The selectivities of CO_2, hydrocarbons, and methanol were also

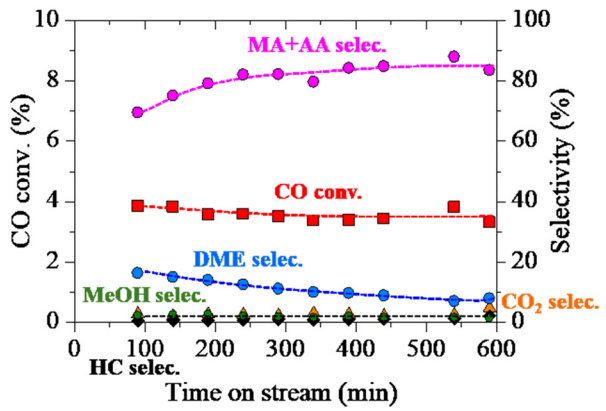

Fig. 1 Time course of CO conversion and product selectivity over the combination of CMYA and Cu(3.1)-MOR(18) catalysts. Reaction conditions: CMYA 0.5 g, Cu(3.1)-MOR(18) 2.5 g, 230 °C, 5 MPa, syngas 150 mL min^{-1}, N_2 50 mL min^{-1}.

stable at approximately 3%, 1%, and 2%, respectively. In contrast, DME selectivity was initially high (17%) but gradually decreased over the first 7 h, reaching a steady value of 8% thereafter. Meanwhile, the combined selectivity of MA and AA increased from 70% at the start to about 85% after 7 h and remained constant out to 10 h. An induction period for MA formation is commonly reported for DME carbonylation over MOR.[15,33,35] The proposed mechanism involves DME reacting with BASs to form methoxy groups, followed by CO insertion to yield acetyl species that react with another DME molecule to form MA, regenerating the methoxy group.[15,18] The observed induction period likely corresponds to the accumulation of surface methoxy species on MOR.

Cu(3.1)-MOR(18) catalyst after reaction was analyzed by TG-MS (Fig. S1). The amount of coke after the 5 h reaction was approximately 3.0 wt% and did not increase with increasing the reaction time to 10 h. This result suggests that coke formation over the Cu-MOR catalyst is not so severe at 230 °C and 5 MPa.

Thus, by loading two types of catalyst in separate layers within a single reactor—a Cu-based catalyst for methanol synthesis on the top and a Cu-exchanged MOR zeolite for DME carbonylation on the bottom—syngas could be selectively converted into MA and AA *via* methanol and DME. The highest total selectivity of MA and AA achieved over the CMYA and Cu-MOR catalyst combination was 85% at a CO conversion of 3.5%.

3.2. Optimization of MOR zeolite catalysts

MOR zeolite was modified with various metal ions, and their catalytic activity for the conversion of syngas to MA and AA was compared (Table 2). The metal ions examined were Zn, Mg, Mn, Co, Fe, Ni, Ag, and Cu, which were loaded onto MOR(18) by ion exchange. The loading amounts varied depending on the type of metal ion but ranged from 1.2 to 4.9 wt% (Table 2). The metal/Al ratio was around 0.30 for most catalysts. The catalytic reaction was conducted under standard conditions (230 °C, 5 MPa, 340 min, 0.5 g CMYA, 2.0 g M-MOR(18), 150 mL min^{-1} syngas, and 50 mL min^{-1} N_2). As noted earlier, the CMYA catalyst alone produced

Table 2 Conversion of syngas to MA and AA over combinations of a CMYA catalyst and a M-MOR(18) zeolite[a]

Entry	Zeolite catalyst	M/Al ratio	CO conv. (%)	Selectivity[b] (%)									Yield of MA + AA (%)
				CO_2	CH_4	C_{2-4} HC	C_{5-6} HC	MeOH	EtOH	MA	AA	DME	
1	Cu catalyst only	—	4.3	0.4	0.5	0.0	0.0	98.6	0.3	0	0.0	0.7	0.00
2	H-MOR(18)	—	4.0	1.7	0.4	0.4	0.0	8.1	0.0	2.1	0.0	86.9	0.08
3	Zn(3.6)-MOR(18)	0.34	3.9	1.7	0.4	0.3	0.0	8.0	0.0	1.5	0.0	89.1	0.06
4	Mg(1.2)-MOR(18)	0.30	4.1	2.0	0.5	0.4	0.0	8.8	0.0	4.2	0.0	84.5	0.17
5	Mn(3.2)-MOR(18)	0.35	3.9	2.4	0.4	0.3	0.0	7.9	0.0	4.5	0.0	83.8	0.18
6	Co(3.0)-MOR(18)	0.31	3.3	1.6	5.7	9.3	2.7	9.2	0.0	5.3	1.5	63.0	0.23
7	Fe(4.7)-MOR(18)	0.52	3.9	2.1	0.5	0.5	0.0	8.1	0.0	10.9	0.0	77.4	0.43
8	Ni(2.0)-MOR(18)	0.21	3.9	6.1	29.8	6.7	1.5	6.5	0.0	10.9	0.9	38.0	0.46
9	Ag(4.9)-MOR(18)	0.28	2.5	4.0	1.0	0.5	0.0	4.9	0.0	41.5	0.0	47.5	1.02
10	Cu(3.1)-MOR(18)	0.30	4.9	8.5	0.4	0.5	0.0	3.4	0.0	60.8	4.0	23.7	3.17

[a] CMYA 0.5 g, M-MOR(18) 2.0 g, 230 °C, 5 MPa, 340 min, syngas 150 mL min^{-1}, N_2 50 mL min^{-1}. [b] C_{2-4} HC: hydrocarbons with a carbon number of 2–4, C_{5-6} HC: hydrocarbons with a carbon number of 5–6, MA: methyl acetate, AA: acetic acid.

methanol with very high selectively (98.6%), while the combination of CMYA and unmodified MOR(18) produced DME with high selectively (86.9%) (Table 1, entries 1 and 2). MA selectivity over these catalysts was 0% and 2.1%, respectively. For the modified MOR zeolites, Zn loading decreased MA selectivity, whereas loading of metals other than Zn increased it. Although Zn has been reported to enhance the catalytic activity of MOR zeolite for DME carbonylation using DME and CO as the reactants,[30,33] it was not effective for syngas conversion to MA and AA using the tandem catalysts. This result may be due to the poisoning of active sites by water. Loading of Mg, Mn, or Fe increased the MA selectivity by a factor of 2–5 without affecting CO_2 or hydrocarbon selectivity (entries 4, 5 and 7). Co-MOR and Ni-MOR exhibited similar MA selectivity to the MOR zeolites loaded with Mg, Mn, or Fe (entries 6 and 8); however, Co and Ni also strongly promoted CH_4 and C_{2-6} hydrocarbon formation, consistent with their known activity in Fischer–Tropsch synthesis and methanation, respectively. Ag-MOR and Cu-MOR exhibited 20–30 times higher MA selectivity than unmodified MOR (entries 9 and 10). This result was surprising because it was reported that loading of Ag or Cu increased the catalytic activity of MOR only by several times in DME carbonylation using DME and CO as the reactants.[13,31] Furthermore, Ag or Cu loading had little influence on hydrocarbon selectivity, although CO_2 selectivity, arising from the water–gas shift reaction, increased by a factor of 2–5. These results clearly indicated that Cu was the most effective promoter for the conversion of syngas to MA and AA in the tandem catalytic system.

The effects of Cu-loading on the selectivity and yield of MA and AA were examined (Table 3, entries 1–8). In this

Table 3 Conversion of syngas to MA and AA over combinations of CMYA and Cu-exchanged zeolite catalysts[a]

Entry	Zeolite catalyst	Cu/Al ratio	CO conv. (%)	Selectivity[b] (%)									Yield of MA + AA (%)
				CO_2	CH_4	C_{2-4} HC	C_{5-6} HC	MeOH	EtOH	MA	AA	DME	
1	Cu catalyst only	—	4.3	0.4	0.5	0.0	0.0	98.6	0.3	0.0	0.0	0.7	0.00
2	H-MOR(18)	—	4.0	1.7	0.4	0.4	0.0	8.1	0.0	2.1	0.0	86.9	0.17
3	Cu(2.4)-MOR(18)	0.23	3.9	1.8	0.7	0.5	0.0	5.8	0.0	46.7	0.0	44.7	1.82
4	Cu(2.7)-MOR(18)	0.25	4.2	3.7	0.5	0.4	0.0	4.1	0.0	56.6	0.6	34.5	2.40
5	Cu(2.9)-MOR(18)	0.27	4.3	2.8	1.0	1.0	0.0	4.5	0.0	52.6	0.0	37.3	2.26
6	Cu(3.1)-MOR(18)	0.30	4.9	8.5	0.4	0.5	0.0	3.4	0.0	60.8	4.0	23.7	3.17
7	Cu(3.3)-MOR(18)	0.31	4.0	4.2	0.4	0.6	0.0	3.3	0.0	64.4	4.3	22.7	2.75
8	Cu(3.7)-MOR(18)	0.36	4.1	2.9	0.5	0.5	0.0	5.1	0.0	54.1	1.1	37.1	2.26
9	Cu(3.0)/MOR(18)[c]	0.29	4.3	5.0	0.9	0.9	0.0	4.8	0.0	47.9	0.4	39.8	2.07
10	Cu(3.4)-MOR(15)	0.28	3.6	7.1	0.5	0.4	0.0	4.9	0.0	49.2	1.5	36.9	1.83
11	Cu(2.4)-MOR(30)	0.37	3.6	2.6	0.4	0.4	0.0	6.3	0.0	33.7	0.0	56.3	1.22
12	Cu(1.2)-MOR(90)	0.52	3.5	2.4	0.3	0.3	0.0	7.9	0.0	10.0	0.0	79.5	0.35
13	Cu(0.4)-MOR(240)	0.50	3.6	0.4	0.4	0.3	0.0	9.1	0.0	3.7	0.0	85.8	0.14
14	Cu(4.2)-CHA(26)	0.57	2.5	1.6	0.4	0.3	0.0	6.8	0.0	22.3	0.0	67.8	0.56
15	Cu(2.7)-FER(18)	0.26	2.9	9.7	0.3	0.2	0.0	5.7	0.0	18.5	0.0	65.4	0.54
16	Cu(3.0)-ZSM-5(24)	0.37	3.7	2.3	0.5	0.4	0.0	8.4	0.0	7.6	0.0	80.4	0.28
17	Cu(2.3)-Beta(25)	0.30	2.7	9.6	0.3	0.9	0.0	6.6	0.0	2.5	0.0	80.7	0.07
18	Cu(5.1)-Y(10)	0.30	3.5	3.9	0.4	0.3	0.0	8.2	0.0	0.3	0.0	85.6	0.01
19	Cu(4.0)-ASA	0.11	3.9	4.3	0.4	0.2	0.0	9.2	0.0	0.0	0.0	86.8	0.00

[a] CMYA 0.5 g, Cu-zeolite 2.0 g, 230 °C, 5 MPa, 340 min, syngas 150 mL min^{-1}, N_2 50 mL min^{-1}. [b] C_{2-4} HC: hydrocarbons with a carbon number of 2–4, C_{5-6} HC: hydrocarbons with a carbon number of 5–6, MA: methyl acetate, AA: acetic acid. [c] The catalyst was prepared by means of an impregnation method.

experiment, Cu-loading was varied by changing the preparation conditions such as the concentration of the $Cu(NO_3)_2$ aqueous solution and the number of ion-exchange steps, yielding six samples with Cu loadings of 2.4–3.7 wt%. CO conversion and C_{1-6} hydrocarbon selectivity remained nearly constant within this range of Cu loading. In contrast, MA and AA selectivity increased with Cu-loading up to 3.3 wt%, then decreased at higher loadings. MeOH and DME selectivity showed the opposite trend, decreasing up to 3.3 wt% and then increasing. The initial increase of MA and AA selectivity with Cu loading is likely due to the greater number of Cu ions accelerating the DME carbonylation rate. However, excessive Cu loading on MOR reduces the number of surface OH groups that work as BASs, slowing methanol dehydration to DME and thereby lowering MA selectivity. The total yield of MA and AA followed a convex upward dependence, reaching its maximum at a Cu loading of 3.1 wt%.

Cu(3 wt%)/MOR(18) prepared by impregnation (Table 3, entry 9) exhibited lower activity than that prepared by ion-exchange with a similar Cu-loading (Cn(3.1)-MOR(18), entry 6), indicating that good dispersion of Cu ions is important for achieving high catalytic activity.

The effects of the SiO_2/Al_2O_3 ratio of the MOR on product selectivity and yield were examined (Table 3, entries 6 and 10–13). Cu was loaded onto five MOR samples with different SiO_2/Al_2O_3 ratios ranging from 15 to 240, and their catalytic activities for syngas conversion to MA and AA were compared. For all catalysts, Cu ion exchange was performed under the same conditions (1 mol L^{-1} $Cu(NO_3)_2$ aqueous solution, ion exchange repeated 3 times). Consequently, Cu loading decreased with increasing SiO_2/Al_2O_3 ratio, which was expected given that zeolites with higher SiO_2/Al_2O_3 ratios have fewer ion-exchange sites. The selectivity and yield of MA and AA increased with SiO_2/Al_2O_3 ratio up to 18, then decreased with further increases. The highest activity was observed for Cu(3.1)-MOR(18) (entry 6). These results indicate that higher Cu loading does not guarantee high DME carbonylation activity, with factors such as the location and oxidation state of the Cu species also playing important roles. Catalytic activity was also evaluated for Cu-exchanged zeolites with different crystal structures and for Cu-exchanged amorphous SiO_2-Al_2O_3 (ASA) (Table 3, entries 6 and 14–19). The tested zeolites were MOR, CHA, FER, ZSM-5, Y, and Beta. MOR has both 8-MR and 12-MR channels; CHA has only 8-MR channels; FER has 8-MR and 10-MR channels; ZSM-5 has 10-MR channels only; and Y and Beta have 12-MR channels only. The Cu loadings for these catalysts ranged from 2.3 to 5.1 wt%. The selectivity and yield of MA and AA followed the order of Cu-MOR > Cu-CHA > Cu-FER > Cu-ZSM-5 > Cu-Beta > Cu–Y > Cu-ASA. It is well known that DME carbonylation efficiently proceeds within the 8-MR channels of unmodified zeolites.[13,16] Similarly, in the tandem system combining a Cu-based catalyst and Cu-exchanged zeolite, zeolites containing 8-MR channels also showed higher activity than those without 8-MR channels, confirming that the reaction proceeds within the 8-MR channels of zeolites.

Thus, Cu(3.1)-MOR(18) was identified as the most effective catalyst for the conversion of syngas to MA and AA using a tandem catalyst system, and this catalyst combination, as well as the other catalysts examined, was subjected to further examination to clarify the origin of its high catalytic activity.

3.3. Characterization of Cu-based catalysts and MOR zeolites

The CMA and CMYA catalysts were characterized by N_2 adsorption, XRD, SEM, H_2-TPR, ICP-AES, and N_2O pulse adsorption. XRD patterns of CMA and CMYA catalysts before H_2 reduction showed peaks at 35.6° and 38.8° (Fig. S2), corresponding to the (002) and (111) crystal planes of CuO (JCPDS Card, No. 48-1548). No diffraction peaks from Mg-, Al-, or Y-containing compounds were observed. SEM images of both catalysts revealed irregularly shaped particles smaller than 10 μm (Fig. S3 a and c). At higher magnification, rod-like particles a few hundred nanometers in size were partially observed in CMYA (red area in Fig. S3d). The BET surface area, pore volume, and average pore size of CMA before H_2 reduction were 105 m^2 g^{-1}, 0.54 cm^3 g^{-1}, and 20.5 nm, respectively, whereas those of CMYA were 201 m^2 g^{-1}, 0.88 cm^3 g^{-1}, and 17.4 nm (Table S2). These results suggest that Y-doping reduced the particle size of CMA. The H_2-TPR profile of CMA showed two reduction peaks centered at 205 and 260 °C, while that of CMYA showed a small shoulder peak at 210 °C and a main peak at 225 °C (Fig. S4A). CMYA showed reduction peaks at lower temperatures than CMA and bulk CuO or Cu_2O (Fig. S4B), indicating that the MgO-Al_2O_3 support and Y-doping reduced Cu particle size and enhanced reducibility. The reduction degrees of Cu on CMA and CMYA, estimated from H_2 consumption below 350 °C, were 87% and 111%, respectively (Table S3), showing that most Cu particles were reduced to metallic Cu during H_2 pretreatment at 350 °C. Cu loading, as measured by ICP-AES, was 38.8 wt% for CMA and 30.5 wt% for CMYA (Table S4). Cu particle sizes measured by N_2O pulse adsorption were 39.6 nm for CMA and 9.9 nm for CMYA, indicating improved Cu dispersion with Y-doping (Table S4). The enhancement of Cu dispersion and reducibility by Y-doping has also been reported by Gao *et al.* for Cu/Zn/Al catalysts.[52]

Next, MOR(18) zeolites ion-exchanged with various metals before H_2 reduction were characterized by N_2 adsorption and XRD. N_2 adsorption results showed that the BET surface area and micropore volume of M-MOR(18) (464–522 m^2 g^{-1} and 0.174–0.194 cm^3 g^{-1}, respectively) were slightly smaller than those of unmodified MOR(18) (522 m^2 g^{-1} and 0.197 cm^3 g^{-1}, respectively) (Table S5, entries 1–9). In contrast, the average pore size of M-MOR(18) (1.93–2.08 nm) was larger than that of MOR(18) (1.83 nm). These results suggest that partial blockage of the micropore entrances by aggregated metal oxide particles after ion exchange led to a decrease of micropore volume and surface area as well as an increase in

average pore size. XRD patterns of M-MOR(18) zeolites exhibited the characteristic diffraction peaks of MOR zeolite (JCPDF Card, No. 43-0171) (Fig. S5).[27,53,54] No diffraction peaks corresponding to the ion-exchanged metal species were observed, indicating that the introduced metal ions were highly dispersed on the MOR zeolite.

Cu-MOR catalysts with different SiO_2/Al_2O_3 ratios were characterized by N_2 adsorption, XRD, and NH_3-TPD. N_2 adsorption results showed that the BET surface area and micropore volume of the Cu-MOR samples were 494–547 $m^2\ g^{-1}$ and 0.187–0.244 $cm^3\ g^{-1}$, respectively, and were generally similar (Table S5, entries 7 and 10–13). However, Cu-MOR zeolites with higher SiO_2/Al_2O_3 ratios, such as Cu-MOR(90) and Cu-MOR(240), exhibited slightly lager total pore volumes and average pore sizes, which may affect the diffusion of reactants and products during the reaction. XRD patterns of Cu-MOR catalysts with different SiO_2/Al_2O_3 ratios showed only peaks corresponding to MOR zeolite, indicating that the Cu species were highly dispersed (data not shown). NH_3-TPD profiles of Cu-MOR zeolites exhibited broad NH_3 desorption signals across the entire temperature range, with decreasing intensity as the SiO_2/Al_2O_3 ratio increased (Fig. S6A). The NH_3-TPD profiles could be deconvoluted into four peaks centered at 200 °C (α peak), 310 °C (β peak), 550 °C (γ peak), and 750 °C (δ peak) (Fig. S6B). The γ peak was attributed to BASs and the δ peak to dehydration of the zeolite framework.[53] The amount of BASs, estimated from the γ peak area, decreased from 1.54 to 0.30 mmol g^{-1} as the SiO_2/Al_2O_3 ratio increased from 15 to 240, suggesting that a Cu-MOR with a moderate amount of BASs would have the highest catalytic activity (Table S6).

The most active of the present catalysts, Cu-MOR(18), was further characterized using UV-vis, FT-IR, H_2-TPR, DRIFTS coupled with CO adsorption, and CO-TPD. The UV-vis spectrum of Cu-MOR(18) before H_2 reduction showed a strong adsorption band at 200–300 nm and weak band at 600–900 nm (Fig. 2). The 200–300 nm band was attributed to charge transfer from framework-coordinated O^{2-} to zeolite-confined Cu^{2+} species (*e.g.*, mononuclear Cu^{2+}, mono(μ-oxo) di-copper, and bis(μ-oxo) di-copper species), while the 600–900 nm band was attributed to d–d transitions of Cu^{2+} in octahedral coordination within the bulk CuO particles.[54–56] Adsorption bands associated with charge transfer from O^{2-} to Cu^{2+} in small CuO clusters (300–500 nm) were not observed. The intensity of the 200–300 nm adsorption band increased with increasing Cu loading, whereas that of the 600–900 nm band remained unchanged. These results indicate that most Cu species occupy ion-exchange sites within the MOR zeolite and maintain high dispersion even at high Cu loadings.

FT-IR spectra in the OH stretching region for unmodified MOR(18) and Cu-MOR(18) with different Cu loadings before H_2 reduction showed OH bands at 3740, 3605, and 3585 cm^{-1} (Fig. 3). According to the literature, the band at 3740 cm^{-1} corresponds to terminal silanol groups on the external surface of MOR, the band at 3605 cm^{-1} to OH groups in the 12-MR channels, and the band at 3585 cm^{-1} to OH groups in the 8-MR channels.[16,23,24,34,35] The intensity of all three bands decreased monotonically with increasing Cu loading,

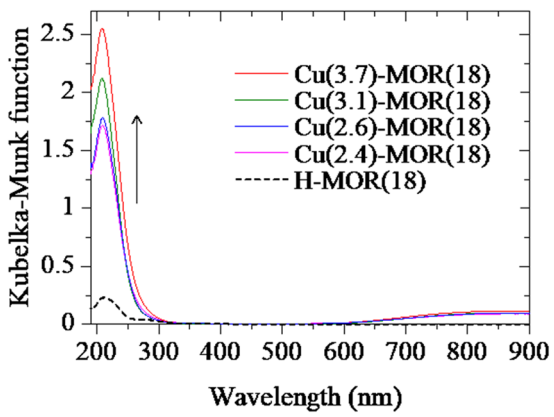

Fig. 2 UV-vis spectra of Cu-MOR(18) zeolites with different Cu-loading before H_2 reduction.

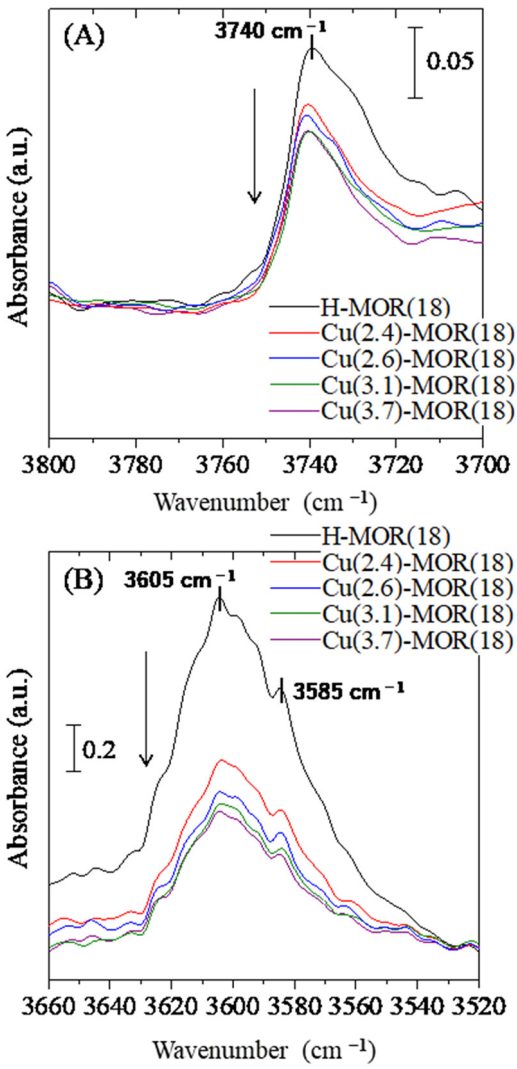

Fig. 3 FT-IR spectra of the O–H stretching region for Cu-MOR(18) zeolites with different Cu loadings before H_2 reduction.

indicating that Cu ions were uniformly distributed over the external surface, 12-MR channels, and 8-MR channels of the MOR zeolite.

H_2-TPR profiles of Cu-MOR(18) showed two reduction peaks centered at around 250 and 575 °C (Fig. 4), consistent with results reported by other research groups.[30,54,56] Assuming that Cu was present as CuO before H_2 reduction, the degree of Cu reduction was roughly estimated from the amounts of H_2 consumed below 350 °C and 800 °C (Table S7). The degrees of reduction at 350 and 800 °C were 61–65% and 97–102%, respectively, and were not affected by Cu loading. These results suggest that Cu^{2+} ions on Cu-MOR(18) were converted to a mixture of Cu^+ ions and metallic Cu after H_2 reduction pretreatment at 350 °C.

DRIFTS spectra of CO adsorbed on unmodified MOR(18) showed no noticeable CO adsorption bands (Fig. 5). In contrast, three bands assigned to CO adsorbed on Cu^+ sites appeared at 2159, 2144, and 2108 cm^{-1} in the spectra of Cu-MOR catalysts after H_2 reduction at 350 °C, indicating that Cu loading greatly enhanced CO adsorption. According to previous reports, the band at 2159 cm^{-1} corresponds to CO adsorbed on Cu^+ ions in 8-MR channels, the band at 2144 cm^{-1} to Cu^+ ions in 12-MR channels, and the band at 2108 cm^{-1} to Cu^+ ions on Cu_2O particles.[27,57–59] In Fig. 5, the relative areas of these three bands were roughly constant, except for Cu(3.4)-MOR(15), with the band at 2159 cm^{-1} accounting for *ca.* 68%, the band at 2144 cm^{-1} for *ca.* 29%, and the band at 2109 cm^{-1} for *ca.* 3%. These results suggest that Cu^+ ions are predominantly located in the 8-MR channels rather than in the 12-MR channels or on the outer surface of MOR.

It is generally accepted that metal–CO bonding involves electron transfer from the CO(5σ) orbital to empty metal orbitals (σ-donation) and from occupied metal orbitals to the CO ($2\pi^*$) orbital (π-back donation).[58] Both the 5σ and $2\pi^*$ orbitals are anti-bonding with respect to the internal C–O bond. Therefore, stronger metal–CO bonding leads to greater π-back donation, which weakens the C–O bond and lowers the CO stretching frequency. In Fig. 5, the C–O stretching frequency of CO adsorbed on Cu^+ ions decreased in the order of 8-MR channels > 12-MR channels > outer surface of MOR, indicating that the Cu^+–CO bond strength increased in the reverse order.

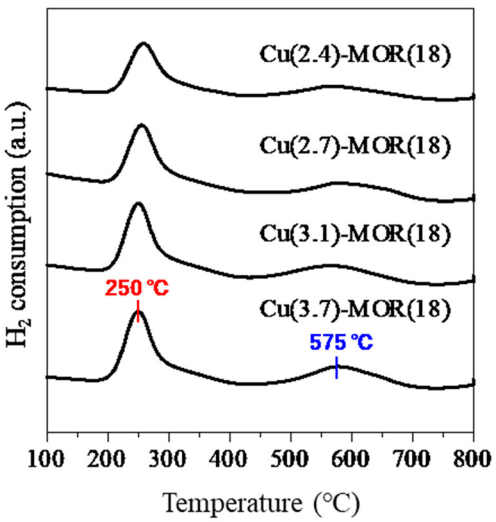

Fig. 4 H_2-TPR profiles of Cu-MOR(18) zeolites with different Cu loadings.

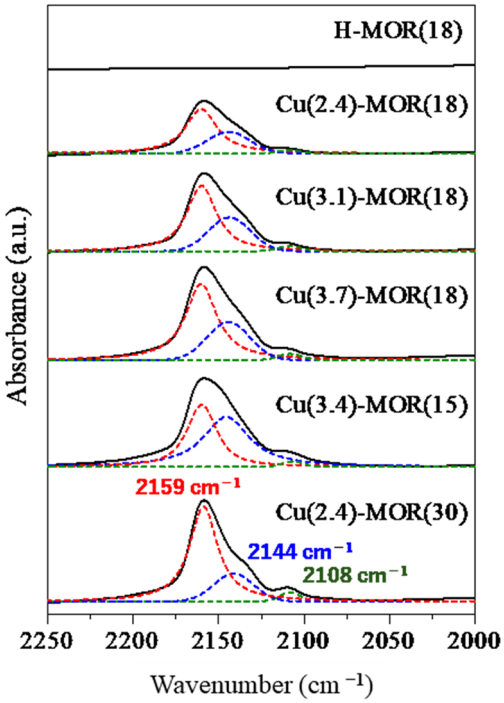

Fig. 5 DRIFTS spectra of CO adsorbed on Cu-MOR(18) zeolites with different Cu loadings.

To examine the reactivity of CO adsorbed on Cu^+ ions, methanol was fed to the CO-adsorbed Cu-MOR zeolite and DRIFT spectra were measured at 100 °C and 0.1 MPa. As the methanol feed time increased, intensity of CO adsorption band at *ca.* 2150 cm^{-1} monotonically decreased (Fig. S7). Instead, intensity of bands at 1700–1350 cm^{-1}, which were characteristic of C=O stretching, C–H bending and C–O stretching vibrations of surface adsorbed acetyl species,[60] increased with increasing the feed time. These results suggest that CO adsorbed on Cu^+ ions would contribute to DME carbonylation.

CO-TPD profiles of unmodified MOR(18) and Cu ion-exchanged MOR zeolites (Fig. 6) showed a similar trend to the DRIFTS spectra of adsorbed CO (Fig. 5). While MOR(18) showed no noticeable CO desorption peaks, three peaks centered at 220, 350, and 780 °C appeared in the profiles of Cu-MOR (Fig. 6), indicating that Cu loading greatly enhanced CO adsorption. Based on the DRIFTS results (Fig. 5), the peaks at 220, 350, and 780 °C were attributed to CO adsorbed on Cu^+ ions in 8-MR channels, in 12-MR channels, and on Cu_2O particles, respectively, as the CO desorption temperature increased with Cu^+–CO bond strength. Notably, the desorption temperature of CO adsorbed on Cu^+ ions in

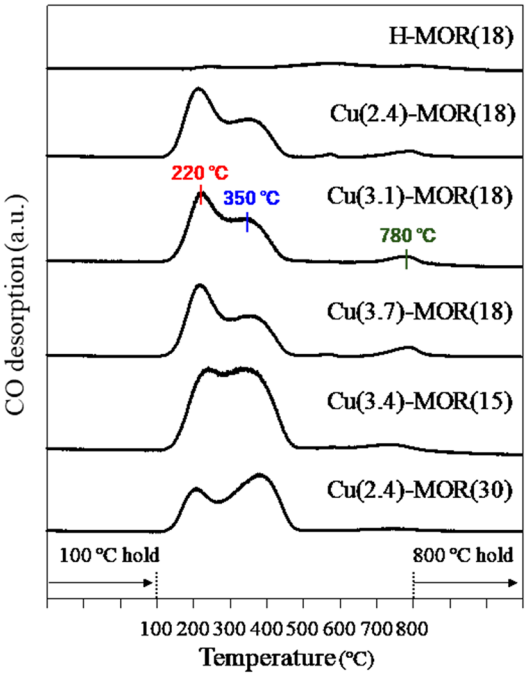

Fig. 6 CO-TPD profiles of Cu-MOR(18) zeolites with different Cu loadings.

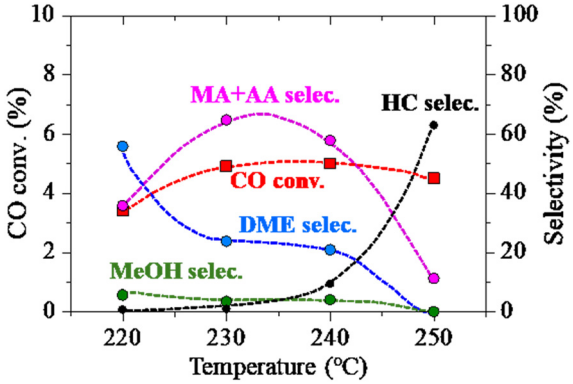

Fig. 7 Effect of reaction temperature on CO conversion and product selectivity over the combination of CMYA and Cu(3.1)-MOR(18) catalysts. Reaction conditions: CMYA 0.5 g, Cu(3.1)-MOR(18) 2.0 g, 220–250 °C, 5 MPa, 340 min, syngas 150 mL min^{-1}, N_2 50 mL min^{-1}.

8-MR channels (220 °C) is close to the reaction temperature for syngas conversion to MA and AA (230 °C), suggesting that these sites play a key role in DME carbonylation. Overall, these results indicate that Cu^+ ions in 8-MR channels promote CO adsorption and insertion into DME, enhancing catalytic activity.

Three types of Cu species, *i.e.*, Cu^{2+},[33] Cu^+,[25,45] and Cu metal,[27,50,51] have been proposed as the active sites of Cu-MOR catalyst for DME carbonylation, and no consensus has been reached. However, our study strongly supports that Cu^+ ions within 8-MR channels work as the active sites for DME carbonylation.

In the CO-TPD profiles of Cu-MOR(18), the amount of CO adsorbed on Cu^+ ions in the 8-MR channels was greater than that adsorbed on Cu^+ ions in the 12-MR channels (Fig. 6). In contrast, Cu-MOR(15) and Cu-MOR(30) showed lower CO adsorption on Cu^+ ions in the 8-MR channels compared to those in the 12-MR channels. Therefore, the high catalytic activity of Cu-MOR(18) (Table 3) may be attributed to the larger proportion of Cu^+ ions located within the 8-MR channels.

3.4. Effects of reaction conditions

To examine the effects of reaction conditions on CO conversion and product selectivity, the reaction temperature was varied in the range of 220–250 °C while keeping other conditions constant (Fig. 7). The reaction was performed using CMYA (0.5 g) and Cu(3.1)-MOR(18) (2.0 g) at 5 MPa, with syngas and N_2 flow rates of 150 and 50 mL min^{-1}, respectively. Increasing the temperature from 220 to 230 °C increased CO conversion from 3.4% to 4.9%, MA selectivity from 35.7% to 60.8%, and AA selectivity from 0% to 4.0% (Table S8), while MeOH and DME selectivities decreased and C_{1-6} hydrocarbon selectivity remained unchanged. This indicates that the temperature increase enhanced methanol synthesis and DME carbonylation rates without promoting DME conversion to hydrocarbons. Further increasing the temperature to 250 °C did not change CO conversion but markedly decreased MA selectivity, while C_{1-6} hydrocarbon selectivity increased, showing that Cu-MOR favors the conversion of DME to C_{1-6} hydrocarbons at temperatures above 230 °C. Furthermore, CO conversion and MA and AA selectivity remained stable over 340 min at 230 °C but declined sharply after 190 min at 250 °C (Fig. S8), with a corresponding increase in hydrocarbon selectivity. CO_2 selectivity also increased with temperature (Table S8), indicating enhanced water–gas shift reaction at higher temperatures. These results indicate that 230 °C was the optimal reaction temperature for selective syngas conversion to MA and AA.

The effects of the weight ratio of Cu catalyst to Cu-MOR zeolite were investigated. CMA was used as the methanol synthesis catalyst, with its amount, reaction temperature, pressure, and syngas/N_2 flow rates fixed at 0.5 g, 230 °C, 5 MPa, 150 mL min^{-1}, and 50 mL min^{-1}, respectively. The amount of Cu(3.1)-MOR(18) was varied from 0 to 3.0 g. Using CMA alone produced methanol with high selectivity, with a CO conversion and methanol selectivity of 3.1% and 97%, respectively (Table S9). When the amount of Cu-MOR was varied in the range 0–3.0 g, CO conversion and C_{1-6} hydrocarbon selectivity remained nearly constant (Fig. 8). Methanol selectivity sharply decreased from 97% to 3.8% as the amount of Cu-MOR was increased from 0 to 0.5 g, and then decreased gradually to 0% with further increases up to 3.0 g. DME selectivity first increased until 0.5 g of Cu-MOR and then decreased with higher amounts. The total selectivity of MA and AA increased steadily with increasing Cu-MOR, indicating that methanol was converted to MA and AA *via*

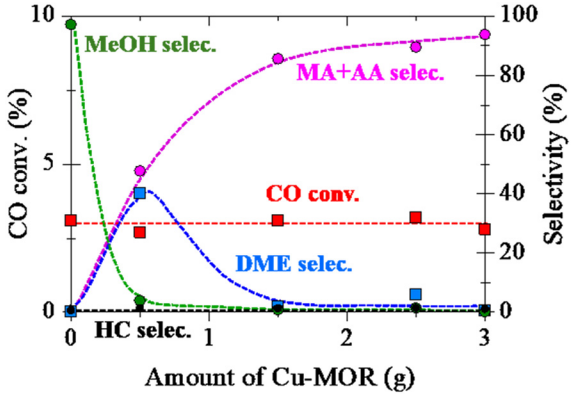

Fig. 8 Effect of the amount of Cu(3.1)-MOR(18) on CO conversion and product selectivity over the combination of CMA and Cu(3.1)-MOR(18) catalysts. Reaction conditions: CMA 0.5 g, Cu(3.1)-MOR(18) 0.0–3.0 g, 230 °C, 5 MPa, 340 min, syngas 150 mL min^{-1}, N_2 50 mL min^{-1}.

DME. These results also showed that Cu-MOR promoted DME carbonylation without enhancing DME-to-hydrocarbon conversion at 230 °C. The total yield of MA and AA reached a maximum of 2.86% at 2.5 g of Cu-MOR, while the total selectivity of MA and AA was highest (93.7%) at 3.0 g of Cu-MOR.

Next, the weight ratio of CMA to Cu(3.1)-MOR(18) was varied from 2.0 g/1.0 g to 0.5 g/2.5 g, while keeping the total catalyst amount constant at 3.0 g. Other conditions were the same as in Fig. 8 and Table S9. As the CMA amount decreased and Cu-MOR increased, CO conversion decreased monotonically (Fig. 9, Table S10), which is reasonable because methanol conversion over CMA slowed with less CMA. Methanol and DME selectivity also decreased steadily, whereas MA and AA selectivity increased with decreasing amount of CMA (*i.e.*, increasing amount of Cu-MOR) because of enhanced DME carbonylation. Similar

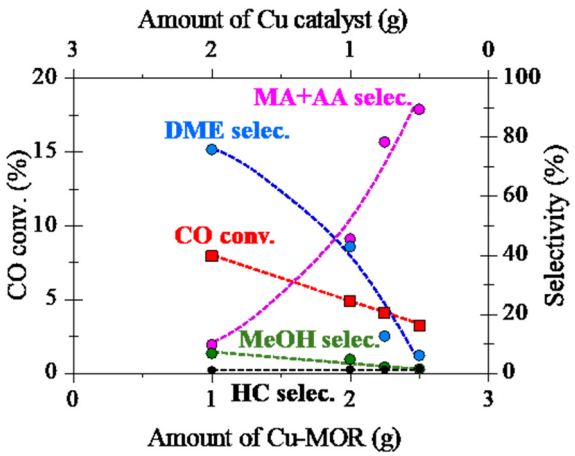

Fig. 9 Effect of CMA/Cu(3.1)-MOR(18) weight ratio on CO conversion and product selectivity over the combination of CMA and Cu(3.1)-MOR(18) catalysts. Reaction conditions: CMA 2.0–0.5 g, Cu(3.1)-MOR(18) 1.0–2.5 g, 230 °C, 5 MPa, 340 min, syngas 150 mL min^{-1}, N_2 50 mL min^{-1}.

to Fig. 8, C_{1-6} hydrocarbon selectivity remained nearly unchanged, indicating a low rate of DME-to-hydrocarbon conversion at 230 °C. The highest total yield of MA and AA (3.22%) was obtained at a CMA/Cu-MOR ratio of 0.75 g/2.25 g, and the highest total selectivity (89.4%) was obtained at a ratio of 0.5 g/2.5 g.

Finally, effects of the gas hourly space velocity (GHSV) were investigated at 230 °C and 5 MPa (Table S11). GHSV was controlled by changing the syngas flow rate from 50 to 200 mL min^{-1}, while keeping the amounts of CMA and Cu-MOR catalysts at 0.5 and 2.5 g. As GHSV was decreased from 4000 to 1000 mL g^{-1} h^{-1}, CO conversion increased slightly from 3.0% to 3.9% due to increasing the contact time of reactants and catalysts. MA and AA selectivity also increased with decreasing GHSV until 2000 mL g^{-1} h^{-1}. However, when GHSV was further decreased to 1000 mL g^{-1} h^{-1}, formation of by-products (*i.e.*, CO_2 and C_{1-6} hydrocarbons) accelerated suddenly and the selectivity of MA and AA decreased. Thus, the highest total selectivity of MA and AA (87.6%) was obtained at 2000 mL g^{-1} h^{-1}.

The optimal reaction conditions in our tandem catalyst setup for selective conversion of syngas to MA and AA were 0.5 g CMA, 3.0 g Cu(3.1)-MOR(18), 230 °C, 5 MPa, with syngas/N_2 flow rates of 150 mL min^{-1} and 50 mL min^{-1}, respectively. Under these conditions, the total selectivity of MA and AA reached 93.7% (Table S9). This value was higher than that of the previously reported tandem catalysts for this reaction (Table S1). The maximum space–time yield (0.67 mmol g^{-1} h^{-1}, Table S9) of our tandem catalyst was also comparable to that of the previously reported tandem catalysts for syngas conversion to ethanol (0.04–6.5 mmol g^{-1} h^{-1}).[48] However, the maximum total yield remained low at 3.2% (Table S10) because of the limited rate of DME carbonylation over Cu-MOR. Increasing the reaction temperature above 230 °C markedly accelerated side reactions, such as DME-to-hydrocarbon conversion and water–gas shift reaction, thereby reducing MA and AA yield (Fig. 7). Therefore, further improvement of yield by simple reaction optimization is expected to be difficult. Developing DME carbonylation catalysts with high activity at low temperatures is required, and our on-going efforts to improve the MOR catalyst will be reported in a future study.

Conclusions

Direct conversion of syngas to MA and AA was investigated using a fixed-bed flow reactor at 230 °C and 5 MPa by coupling a Cu-based methanol synthesis catalyst with a zeolite-based DME carbonylation catalyst. Cu-based complex oxide catalysts containing Cu, Mg, Y, and Al converted syngas to methanol with high selectivity (>97%), while metal ion-exchanged zeolites selectively converted methanol to MA and AA *via* DME. High selectivity for MA and AA was achieved by the sequential action of these catalysts. The catalytic performance of the metal ion-exchanged zeolites varied markedly with the type of metal ion and zeolite structure,

with Cu-MOR showing the highest activity. Cu-MOR activity was also influenced by Cu loading and the SiO_2/Al_2O_3 ratio of MOR; catalysts with moderate Cu loading and SiO_2/Al_2O_3 ratio showed optimal performance, indicating cooperative effects between Cu and the BASs of MOR for DME carbonylation. Characterization of Cu-MOR by N_2 adsorption, XRD, NH_3-TPD, UV-vis, FT-IR, H_2-TPR, DRIFTS with CO adsorption, and CO-TPD suggested that Cu^+ ions within 8-MR channels strongly promoted CO adsorption and insertion into DME, leading to high catalytic activity. The reaction conditions also affected performance, with the highest total selectivity of MA and AA (93.7%) achieved at 230 °C, a Cu catalyst/Cu-MOR weight ratio of 1 : 6, and a gas hourly space velocity of 3.4 L g^{-1} h^{-1}. However, the maximum total yield remained low at 3.2%. This study highlights that control of the amount, oxidation state, and location of ion-exchanged Cu ions is crucial for developing more active Cu-MOR catalysts for DME carbonylation.

Author contributions

Katsuya Shimura: methodology, investigation, writing–original draft. Isao Nakamura: conceptualization, project administration, supervision, writing–review & editing. Tadahiro Fujitani: conceptualization, project administration, supervision, writing–review & editing.

Conflicts of interest

There are no conflicts to declare.

Data availability

The data supporting this article have been included as part of the supplementary information (SI).

Supplementary information: experimental procedures, characterization data, supplementary tables and figures. See DOI: https://doi.org/10.1039/d6cy00105j.

Acknowledgements

The authors are deeply grateful to Yukihiro Nakayama and Makiko Yanagida for their experimental assistance.

References

1 Ö. Tezer, N. Karabağ, A. Öngen, C.Ö. Çolpan and A. Ayol, *Int. J. Hydrogen Energy*, 2022, **47**, 15419–15433.
2 G. Lopez, M. Artetxe, M. Amutio, J. Alvarez, J. Bilbao and M. Olazar, *Renewable Sustainable Energy Rev.*, 2018, **82**, 576–596.
3 S. Rönsch, J. Schneider, S. Matthischke, M. Schlüter, M. Götz, J. Lefebvre, P. Prabhakaran and S. Bajohr, *Fuel*, 2016, **166**, 276–296.
4 M. J. da Silva, *Fuel Process. Technol.*, 2016, **145**, 42–61.
5 V. Dieterich, A. Buttler, A. Hanel, H. Spliethoff and S. Fendt, *Energy Environ. Sci.*, 2020, **13**, 3207–3252.
6 J. Sun and Y. Wang, *ACS Catal.*, 2014, **4**, 1078–1090.
7 L. He, B. Zhou, D. Sun, W. Li, W. Lv, J. Wang, Y. Liang and A. Lu, *ACS Catal.*, 2023, **13**, 11291–11304.
8 X. Li, Y. Zhao, J. Pang, P. Gao, M. Zheng and G. Hou, *ACS Catal.*, 2025, **15**, 5053–5085.
9 H. T. Luk, C. Mondelli, D. C. Ferré, J. A. Stewart and J. Pérez-Ramírez, *Chem. Soc. Rev.*, 2017, **46**, 1358–1426.
10 G. Liu, G. Yang, X. Peng, J. Wu and N. Tsubaki, *Chem. Soc. Rev.*, 2022, **51**, 5606–5659.
11 S. Liu, D. Wu, Y. Zhao, Y. Liang, L. Zhang, J. Sun, J. Lin, S. Wang, Y. Yao, S. Wan, N. J. Coville, Y. Wang and H. Xiong, *Energy Fuels*, 2024, **38**, 14769–14796.
12 J. Kang, S. He, W. Zhou, Z. Shen, Y. Li, M. Chen, Q. Zhang and Y. Wang, *Nat. Commun.*, 2020, **11**, 827.
13 E. Zhan, Z. Xiong and W. Shen, *J. Energy Chem.*, 2019, **36**, 51–63.
14 P. Cheung, A. Bhan, G. J. Sunley and E. Iglesia, *Angew. Chem., Int. Ed.*, 2006, **45**, 1617–1620.
15 P. Cheung, A. Bhan, G. J. Sunley, D. J. Law and E. Iglesia, *J. Catal.*, 2007, **245**, 110–123.
16 A. Bhan, A. D. Allian, G. J. Sunley, D. J. Law and E. Iglesia, *J. Am. Chem. Soc.*, 2007, **129**, 4919–4924.
17 M. Boronat, C. Martínez-Sánchez, D. Law and A. Corma, *J. Am. Chem. Soc.*, 2008, **130**, 16316–16323.
18 M. Boronat, C. Martínez and A. Corma, *Phys. Chem. Chem. Phys.*, 2011, **13**, 2603–2612.
19 D. B. Rasmussen, J. M. Christensen, B. Temel, F. Studt, P. G. Moses, J. Rossmeisl, A. Riisager and A. D. Jensen, *Catal. Sci. Technol.*, 2017, **7**, 1141–1152.
20 Z. Liu, X. Yi, G. Wang, X. Tang, G. Li, L. Huang and A. Zheng, *J. Catal.*, 2019, **369**, 335–344.
21 B. Li, J. Xu, B. Han, X. Wang, G. Qi, Z. Zhang, C. Wang and F. Deng, *J. Phys. Chem. C*, 2013, **117**, 5840–5847.
22 T. He, X. Liu, S. Xu, X. Han, X. Pan, G. Hou and X. Bao, *J. Phys. Chem. C*, 2016, **120**, 22526–22531.
23 H. Zhou, W. Zhu, L. Shi, H. Liu, S. Liu, Y. Ni, Y. Liu, Y. He, S. Xu, L. Li and Z. Liu, *J. Mol. Catal. A: Chem.*, 2016, **417**, 1–9.
24 A. A. C. Reule, J. A. Sawada and N. Semagina, *J. Catal.*, 2017, **349**, 98–109.
25 T. Blasco, M. Boronat, P. Concepción, A. Corma, D. Law and J. A. Vidal-Moya, *Angew. Chem., Int. Ed.*, 2007, **46**, 3938–3941.
26 H. Xue, X. Huang, E. Ditzel, E. Zhan, M. Ma and W. Shen, *Ind. Eng. Chem. Res.*, 2013, **52**, 11510–11515.
27 H. Zhan, S. Huang, Y. Li, J. Lv, S. Wang and X. Ma, *Catal. Sci. Technol.*, 2015, **5**, 4378–4389.
28 H. Zhou, W. Zhu, L. Shi, H. Liu, S. Liu, S. Xu, Y. Ni, Y. Liu, L. Li and Z. Liu, *Catal. Sci. Technol.*, 2015, **5**, 1961–1968.
29 M. Ma, E. Zhan, X. Huang, N. Ta, Z. Xiong, L. Bai and W. Shen, *Catal. Sci. Technol.*, 2018, **8**, 2124–2130.
30 A. A. C. Reule, V. Prasad and N. Semagina, *Microporous Mesoporous Mater.*, 2018, **263**, 220–230.
31 S. Li, K. Cai, Y. Li, S. Liu, M. Yu, Y. Wang, X. Ma and S. Huang, *ChemCatChem*, 2020, **12**, 3290–3297.
32 H. Sheng, H. Ma, W. Qian, N. Fei, H. Zhang and W. Ying, *Energy Fuels*, 2019, **33**, 10159–10166.
33 S. Wang, W. Guo, L. Zhu, H. Wang, K. Qiu and K. Cen, *J. Phys. Chem. C*, 2015, **119**, 524–533.

34 H. Xue, X. Huang, E. Zhan, M. Ma and W. Shen, *Catal. Commun.*, 2013, **37**, 75–79.
35 K. Cao, D. Fan, L. Li, B. Fan, L. Wang, D. Zhu, Q. Wang, P. Tian and Z. Liu, *ACS Catal.*, 2020, **10**, 3372–3380.
36 R. Liu, S. Zeng, T. Sun, S. Xu, Z. Yu, Y. Wei and Z. Liu, *ACS Catal.*, 2022, **12**, 4491–4500.
37 R. Liu, B. Fan, W. Zhang, L. Wang, L. Qi, Y. Wang, S. Xu, Z. Yu, Y. Wei and Z. Liu, *Angew. Chem., Int. Ed.*, 2022, **61**, e202116990.
38 D. Fan, N. Chen, S. Han, L. Li, N. Wang, W. Cui, Q. Wang, P. Tian and Z. Liu, *ACS Appl. Mater. Interfaces*, 2024, **16**, 18745–18753.
39 X. Li, X. San, Y. Zhang, T. Ichii, M. Meng, Y. Tan and N. Tsubaki, *ChemSusChem*, 2010, **3**, 1192–1199.
40 G. Yang, X. San, N. Jiang, Y. Tanaka, X. Li, Q. Jin, K. Tao, F. Meng and N. Tsubaki, *Catal. Today*, 2011, **164**, 425–428.
41 P. Lu, G. Yang, Y. Tanaka and N. Tsubaki, *Catal. Today*, 2014, **232**, 22–26.
42 Q. Wei, G. Yang, X. Gao, L. Tan, P. Ai, P. Zhang, P. Lu, Y. Yoneyama and N. Tsubaki, *Chem. Eng. J.*, 2017, **316**, 832–841.
43 W. Zhou, J. Kang, K. Cheng, S. He, J. Shi, C. Zhou, Q. Zhang, J. Chen, L. Peng, M. Chen and Y. Wang, *Angew. Chem., Int. Ed.*, 2018, **57**, 12012–12016.
44 Z. Cao, T. Hu, J. Guo, J. Xie, N. Zhang, J. Zheng, L. Che and B. H. Chen, *Fuel*, 2019, **254**, 115542.
45 Y. Zhang, C. Ding, J. Wang, Y. Jia, Y. Xue, Z. Gao, B. Yu, B. Gao, K. Zhang and P. Liu, *Catal. Sci. Technol.*, 2019, **9**, 1581–1594.
46 D. C. Upham, M. Orazov and T. F. Jaramillo, *J. Catal.*, 2021, **399**, 132–141.
47 W. C. Sung, H. S. Jung, J. W. Bae, J. Y. Kim and D. H. Lee, *J. CO_2 Util.*, 2023, **69**, 102411.
48 S. Han, D. Fan, N. Chen, W. Cui, L. He, P. Tian and Z. Liu, *ACS Catal.*, 2023, **13**, 10651–10660.
49 S. Liu, G. Wu, Y. Chen, Y. Han, M. Zhang, J. Kang, M. Tang, K. P. de Jong, Q. Zhang, Y. Wang and K. Cheng, *AIChE J.*, 2025, **71**, e18664.
50 Y. Li, S. Huang, Z. Cheng, S. Wang, Q. Ge and X. Ma, *J. Catal.*, 2018, **365**, 440–449.
51 S. Wang, S. Li, L. Zhang, Z. Qin, Y. Chen, M. Dong, J. Li, W. Fan and J. Wang, *Catal. Sci. Technol.*, 2018, **8**, 3193–3204.
52 P. Gao, F. Li, N. Zhao, F. Xiao, W. Wei, L. Zhong and Y. Sun, *Appl. Catal., A*, 2013, **468**, 442–452.
53 Y. Liu, J. Qi, K. Zhu, H. Liu, X. Liu, M. Wang, M. Wang, J. Lv, S. Huang and X. Ma, *Catal. Sci. Technol.*, 2025, **15**, 2510–2518.
54 H. Lv, S. Meng, Z. Cui, S. Li, D. Li, X. Gao, H. Guo, A. Bogaerts and Y. Yi, *Chem. Eng. J.*, 2024, **496**, 154337.
55 G. Brezicki, J. Zheng, C. Paolucci, R. Schlögl and R. J. Davis, *ACS Catal.*, 2021, **11**, 4973–4987.
56 M. Picinini, M. G. dos Santos, J. M. C. Bueno and E. A. Urquieta-Gonzalez, *Mol. Catal.*, 2025, **579**, 115093.
57 C. Lamberti, S. Bordiga, A. Zecchina, M. Salvalaggio, F. Geobaldo and C. O. Areán, *J. Chem. Soc., Faraday Trans.*, 1998, **94**, 1519–1525.
58 N. D. Nielsen, T. E. L. Smitshuysen, C. D. Damsgaard, A. D. Jensen and J. M. Christensen, *Surf. Sci.*, 2021, **703**, 121725.
59 H. Xie, D. Yi, L. Shi and X. Meng, *Chem. Eng. J.*, 2017, **313**, 663–670.
60 L. A. Luque-Álvarez, G. Torres-Sempere, F. Romero-Sarria, L. F. Bobadilla, T. Ramírez-Reina and J. A. Odriozola, *Microporous Mesoporous Mater.*, 2024, **378**, 113258.